Available online at www.sciencedirect.com
SCIENCE DIRECT®
Journal of Magnetic Resonance 167 (2004) 147–160
JMR Journal of Magnetic Resonance
www.elsevier.com/locate/jmr

On the philosophy of optimizing contrast agents. An analysis of ^{1}H NMRD profiles and ESR lineshapes of the Gd(III)complex MS-325 + HSA

Xiangzhi Zhou,[a] Peter Caravan,[b] R.B. Clarkson,[c] and Per-Olof Westlund[a,*]

[a] *Department of Bio-physical Chemistry, Umeå University, SE-901 87 UMEÅ, Sweden*
[b] *EPIX Medical, Inc., 71 Rogers Street, Cambridge, MA 02142-1118, USA*
[c] *College of Veterinary Medicine, Illinois EPR Research Center, University of Illinois at Urbana-Champaign, Urbana 61874, USA*

Received 18 June 2003; revised 7 November 2003

Abstract

A generalization of the modified SBM theory is developed in closed analytical form. The theory is applied to describe the paramagnetically enhanced water proton spin–lattice relaxation rates of the aqueous-systems containing a gadolinium($S = 7/2$) complex(MS-325) in the presence or absence of human serum albumin (HSA). MS-325 binds to HSA: in the absence of the protein the reorientational time, τ_R, is short, but when HSA is added τ_R becomes much longer. In this way, the effect of reorientational motion, static (Δ_s), and transient (Δ_t) zero-field splitting (ZFS) interactions on both the water proton relaxivity and the Gd ESR lineshapes are investigated.

Two dynamic models of electron spin relaxation are presented, characterized by transient and static ZFS-interactions. X-, Q-, and W-bands ESR spectra of MS-325+HSA are analyzed in order to describe the effect on the electron spin system upon binding to a macromolecule. A computer program based on this theory is developed which calculates solvent water proton T_1 NMRD profiles and the corresponding X-, Q-, U-, and W-bands ESR lineshapes.

1. Introduction

NMR-paramagnetic relaxation enhancement (PRE) refers to the enhancement of NMR relaxation rates of solvent water protons in the vicinity of the paramagnetic species. The effects of paramagnetic ions on NMR relaxation rates have found important application in studies of metal ions in biochemical systems [1] and as contrast agents in MRI studies [2]. The PRE-theory of paramagnetic hexa-aquo metal ion complexes is well described for most cases by the traditional PRE theory which is due to Solomon, Bloembergen, and Morgan (SBM) [3,4]. An important exception, when the SBM theory fails, is for paramagnetic complexes with very fast electron spin relaxation such as Ni^{2+}aquo complexes [5,6]. However, for other paramagnetic aquo complexes complications such as a change in the water coordination symmetry may make the application of the SBM theory doubtful. Paramagnetic hexa-aquo metal ions complexes, $M^{n+}(H_2O)_6$, are expected to become perturbed by the anisotropic interaction at a macromolecule interface. This perturbation may slow down the dynamics of the water shell, and consequently the modulation of the zero-field splitting (ZFS) interaction, and it may reduce the water coordination number $q < 6$. The anisotropy of the fluctuating ZFS-interaction may thus introduce a reorientational modulated 'static' ZFS-iteraction. These are complications that were not fully taken into account by the traditional SBM theory.

The micro-heterogeneous character of macromolecular systems is thus expected to introduce at least two different timescales, a slow and a fast modulation of the electron spin–lattice coupling. It is therefore reasonable that ZFS-interaction is described in terms of a *transient* and a *static* part.

The reduction of the water coordination number of the paramagnetic metal ion reduces the PRE effect most

* Corresponding author. Fax: +46-90-785-77-79.
E-mail address: per-olof.westlund@chem.umu.se (P.-O. Westlund).

1090-7807/$ - see front matter © 2003 Elsevier Inc. All rights reserved.
doi:10.1016/j.jmr.2003.12.006

drastically but may also introduce changes of the electron spin levels through the static ZFS-interaction. These are problems which were recognized 30 years ago by Dwek in his discussion of paramagnetic ions used in studies of biochemical systems [7]. The critical discussion by Burton et al. [8] focused on the parameters obtained using the SBM theory in biochemical/macromolecular systems. However, no theoretical alternative to the SBM-equations was available at that time.

In the 1980s a generalized PRE theory was developed by a Stockholm group in order to explain PRE data of low-symmetric Ni(II) complexes [9]. In the high field regime, the Ni^{2+} aquo-complex was particularly interesting because it was not possible to observe this complex by conventional ESR spectroscopy. The theoretical approach is very general and applicable to all types of systems and magnetic field strengths. It accounts for low as well as for high field PRE-data and multi-exponential electron spin relaxation within as well as outside the second order perturbation regime. The SBM theory is readily extracted from this general formulation using second order perturbation theory. The theoretical framework is however rather complex. It is based on the stochastic Liouville equation in the Fokker–Planck form, in which the electron spin system is described implicitly. It is therefore not possible to interpret the NMRD-results in terms of electron spin relaxation rates but only in terms of more fundamental parameters. Comparison between SBM and this slow-motion theory has been performed by comparing NMRD profiles, displaying large discrepancies mainly at low fields. The slow-motion approach has also been generalized to low-symmetry complexes of higher electron spin quantum number $S > 1$ [10–13] and it has been reviewed twice [5,6].

During the same time period a new approximate PRE theory was developed by a Florence group [14–20]. This approach was motivated by a number of new experimental water proton T_1-NMRD profiles [21] obtained from studies of paramagnetic metal ions in aqueous solution or/and bound to macromolecule. This low-field theory describes electron spin relaxation on a phenomenological level using two relaxation times T_{1e} and T_{2e}. However, improved phenomenological models were also developed which accounted for low-symmetry coordination of high spin metal ions. In other words a static low-symmetry coordination was assumed to generate a static ZFS-interaction which thus was allowed to modify the electron spin levels. The main flaw of this approach was the absence of a detailed microscopic description of the electron spin relaxation times T_{1e} and T_{2e}.

In the 1990s the research group of R. Sharp also presented an approximate PRE approach based on a phenomenological description of the electron spin system. This approach resembled, at the beginning, very much the low-field approach developed by the Florence group. However, new systems and new PRE data were produced and analyzed using a developed theory and an approximate computational approach [22–38].

Recently, a Swiss and French group [39–41] has contributed to this field by combining ESR studies of paramagnetic contrast agents (mainly Gd-chelates) with water T_1-NMRD profile measurements. Rast et al. [39,40] developed a general method based on Redfield's approximation by introducing the combined effects of the modulation of the static crystal field and the transient ZFS, which interpreted the full electron paramagnetic resonance lineshapes of Gd^{3+} complexes in solution at multiple temperatures and frequencies.

More recent developments by Kowalewski and coworkers [42–46] have been focused on detail in the electron Hamiltonians such as rombicity, special effects in the low-field region. Dynamic models covering slow and fast motion effects have been analyzed within the Stochastic Liouville approach. They have also tried to bring the Florence and the Stockholm approaches together. A very informative review on this recent theoretical development has been published by Kowalewski et al. [47].

A main restriction of the SBM theory is that it ignores multiexponential electron spin relaxation effects. For high electron spin quantum numbers $S > 1$, in the second order perturbation regime and non-extreme narrowing conditions, multiexponential electron spin relaxation is expected. It is thus important at high fields and for slow modulation of ZFS-interaction. That is, for superconducting NMR spectrometers and for MRI studies with slow tumbling low-symmetry contrast agents. This problem was solved numerically more than 30 years ago [48] for $S = 3/2$ and $S = 5/2$ and deprived the SBM equations of their very simple closed form. Perhaps because of this, these results had very little influence on the popularity of the traditional SBM equations as the main tool in the analyses of experimental PRE-data. Quite recently multiexponential electron spin relaxation has been accounted for in new expressions in closed form [49,53,54] and in alternative numerical approaches [41] however still not changing the popularity of the simple SBM theory.

The low-field regime of the water T_1-NMRD profiles introduced an extra complication which also calls SBM in question. This problem has also been solved in a new low-field approach using Redfield theory [55–58].

1.1. The aim and scope of this work

A common philosophy of how to improve and optimize paramagnetic contrast agents is to introduce chemical modification in order to increase the reorientational correlation time, without decreasing the hydration number q. However, upon such a modification

one may also introduce a perturbation which introduces a static ZFS-interaction Δ_s. The latter influences both the electron spin levels and the electron spin relaxation rates of the system. The static ZFS-interaction is modulated by the reorientation and thus a slow tumbling complex may increase its electron spin relaxation rates. The electron spin–spin relaxation rate is most sensitive to this reorientational modulated static ZFS-interaction. An increase in Δ_s may thus counterbalance the improvement in relaxivity due to an increase in τ_R. But it is expected that this enhanced electron spin relaxation is most important at an intermediate field region where both electron T_1 and T_2 processes are important for the NMRD profile. At high fields where the electron spin–lattice relaxation rates are dominant this effect becomes less important. This is the problem investigated in this work. We develop the generalized SBM theory (GSBM) for low-symmetry complexes of spin quantum number $S = 7/2$ and which accounts for multiexponential electron spin relaxation, and describes water T_1-NMRD profiles and corresponding ESR lineshapes. We derive the ESR lineshape function of an $S = 7/2$ ion within the same Hamiltonian defining the NMRD experiment. The approach is based on previous publications [53,54] but which were limited to symmetric Gd-complexes.

Within this theoretical framework we focus on the enhanced proton T_1 spin–lattice relaxation rate of modified Gd-DTPA complexes namely MS-325 and MS-325 + HSA. We relate, in detail, the water relaxivity to the reorientational correlation time τ_R (for instance modified by attaching the chelate to a macromolecule), to the change in the flexibility of the Gd-ion environment, measured by the transient ZFS-interaction, Δ_t and to the averaged symmetry of the Gd-complex measured by the size of the static ZFS-interaction Δ_s. Assuming no changes in the water coordination number q, we investigate both ESR-line width and NMRD-profiles. The theoretical model is used to analyze both the NMRD profiles and the corresponding ESR lineshapes of a contrast agent, MS-325 and MS-325 + HSA within the same dynamic model. Two different dynamic models are introduced in order to describe the flexibility of the Gd(III) environment in the two complexes.

Model I considers rotational diffusion of the paramagnetic complex in the static limit averaging over angle-dependent electron spin relaxation. This dynamic model is thus appropriate for the slow-tumbling MS-325 + HSA complex. The electron spin relaxation is described at fixed orientations of the paramagnetic complex. The transient ZFS-interaction on the other hand is modeled using an anisotropic pseudo-rotation model. Electron spin relaxation thus becomes angle dependent and the ESR spectra is obtained after averaging over all orientations. The model parameters which determine the electron spin relaxation are the following: the transient ZFS-interaction Δ_t^{ZFS}, the pseudo-rotation correlation times $\tau_\perp$ and $\tau_\parallel$ and the static ZFS Δ_s^{ZFS}, which only influences the electron spin levels.

In **model II** the reorientational diffusion motion is allowed to modulate the static ZFS-interaction which thus becomes an important electron spin relaxation mechanism. This model is designed to describe tumbling low-symmetry complexes such as Gd-DTPA and MS-325. The model has the following model parameters: the transient ZFS-interaction Δ_t^{ZFS}, the static ZFS-interaction Δ_s^{ZFS}, one pseudo-rotation correlation time τ_f and the reorientation correlation time τ_R.

Other model parameters are the same for both models and influence the NMRD profile in the same way. These parameters are: the water coordination number q, the concentration of paramagnetic ions m, the rotational diffusion correlation time τ_R, the inner-sphere water residency time τ_M and the average distance between the water proton and the electron spin of the Gd-ion(r_{IS}).

2. Theoretical approach

The inner sphere water proton relaxivity $1/T_{1p}M$, is expressed as the relaxation enhancement divided by the concentration of paramagnetic ions, measured in units of $(\mathrm{mMs})^{-1}$. The inner-sphere relaxivity is given by

$$\frac{1}{T_{1p}M} = \left(\frac{q \cdot 10^{-3}}{55.56}\right)\frac{1}{T_{1M} + \tau_M}, \tag{1}$$

where q denotes the number of fast exchanging water molecules in the first hydration shell of a paramagnetic metal ion with electron spin quantum number S. M and 55.6 are molar concentrations of paramagnetic ions and water, respectively. τ_M is the mean residence lifetime of the inner sphere water and T_{1M} is the spin–lattice relaxation time of the above inner sphere water molecules. Considering only the relaxation contribution due to nuclear spin–electron spin dipole–dipole interaction, the paramagnetically enhanced proton spin–lattice relaxation time T_{1M} is expressed as

$$\frac{1}{T_{1M}} = \frac{4}{3}\left(\frac{\mu_0}{4\pi}\right)^2 \hbar^2 \gamma_I^2 \gamma_S^2 \frac{S(S+1)}{r_{IS}^6}\tau_c^{DD}, \tag{2}$$

where dipole–dipole correlation time τ_c^{DD} is defined as a weighted sum of spectral density functions s_σ^{DD}, σ represents −1, 0, +1.

$$\tau_c^{DD} = Re\left(0.1 \times s_1^{DD} + 0.3 \times s_0^{DD} + 0.6 \times s_{-1}^{DD}\right), \tag{3}$$

where s_σ^{DD} is the Fourier–Laplace transform of the reorientation correlation function and the electron spin correlation function $tr_S\{S_\sigma^{1\dagger} e^{i\hat{L}_S\tau} S_\sigma^1 \rho_S^T\}$ at the nuclear Larmor frequency ω_I.

$$\begin{aligned} s_\sigma^{DD} &= \frac{3}{S(S+1)}\int_0^\infty tr_S\left\{S_\sigma^{1\dagger} e^{i\hat{L}_S\tau} S_\sigma^1 \rho_S^T\right\} e^{-(i\omega_I + 1/\tau_R)\tau}\, d\tau \\ &\equiv M_{\sigma\sigma}^{-1} \end{aligned} \tag{4}$$

Here $M_{\sigma\sigma}^{-1}$ is an inverted matrix element (see Appendix A) and the superoperator is indicated by a 'hat' $\hat{L}$ whereas a spin operator is written without.

2.1. The relation to the Solomon–Bloembergen–Morgan theory

Eq. (4) describes the effective dipole–dipole correlation time and it simplifies to a sum of relaxation rates in the traditional SBM theory because the electron spin–spin and spin–lattice relaxation are single exponential.

$$\begin{aligned} s_1^{\mathrm{DD}} &\to \frac{1}{(\mathrm{i}\omega_\mathrm{I} - \mathrm{i}\omega_\mathrm{S} + 1/T_{2\mathrm{S}} + 1/\tau_\mathrm{R})} = \frac{\tau_{c2}}{(\mathrm{i}(\omega_\mathrm{I} - \omega_\mathrm{S})\tau_{c2} + 1)}, \\ s_0^{\mathrm{DD}} &\to \frac{1}{(\mathrm{i}\omega_\mathrm{I} + 1/T_{1\mathrm{S}} + 1/\tau_\mathrm{R})} = \frac{\tau_{c1}}{(\mathrm{i}\omega_\mathrm{I}\tau_{c1} + 1)}, \\ s_{-1}^{\mathrm{DD}} &\to \frac{1}{(\mathrm{i}\omega_\mathrm{I} + \mathrm{i}\omega_\mathrm{S} + 1/T_{2\mathrm{S}} + 1/\tau_\mathrm{R})} = \frac{\tau_{c2}}{(\mathrm{i}(\omega_\mathrm{I} + \omega_\mathrm{S})\tau_{c2} + 1)}, \end{aligned} \tag{5}$$

where we have introduced two effective correlation times

$$\begin{aligned} \frac{1}{\tau_{c2}} &= 1/T_{2\mathrm{S}} + 1/\tau_\mathrm{R}, \\ \frac{1}{\tau_{c1}} &= 1/T_{1\mathrm{S}} + 1/\tau_\mathrm{R}. \end{aligned} \tag{6}$$

The electron spin relaxation rates $1/T_{1\mathrm{S}}$ and $1/T_{2\mathrm{S}}$ are expressed in terms of spectral densities using Redfield theory:

$$\begin{aligned} \frac{1}{T_{1\mathrm{S}}} = \frac{[4S(S+1)-3]}{25}\{ & \Delta_\mathrm{t}^2\tau_\mathrm{f}\big(1/(1+\omega_\mathrm{s}^2\tau_\mathrm{f}^2) \\ & + 4/\big(1+4\omega_\mathrm{S}^2\tau_\mathrm{f}^2\big)\big) + \Delta_\mathrm{S}^2\tau_\mathrm{R}\big(1/\big(1+\omega_\mathrm{S}^2\tau_\mathrm{R}^2\big) \\ & + 4/(1+4\omega_\mathrm{S}^2\tau_\mathrm{R}^2)\big)\}, \end{aligned} \tag{7}$$

$$\begin{aligned} \frac{1}{T_{2\mathrm{S}}} = \frac{1}{2}\frac{1}{T_{1\mathrm{S}}} + \frac{[4S(S+1)-3]}{50}\{ & \Delta_\mathrm{t}^2\tau_\mathrm{f}\big(3+4/\big(1+\omega_\mathrm{S}^2\tau_\mathrm{f}^2\big)\big) \\ & + \Delta_\mathrm{S}^2\tau_\mathrm{R}\big(3+4/\big(1+\omega_\mathrm{S}^2\tau_\mathrm{R}^2\big)\big)\}, \end{aligned} \tag{8}$$

The dynamic model **II** used in Eqs. (7) and (8) assumes a fast distortion motion of the Gd(III) ion environment causing a transient ZFS-interaction(Δ_t) and a reorientational modulated static ZFS-interaction(Δ_s). The SBM theory is thus given by Eqs. (5)–(8) together with Eqs. (2) and (3).

2.2. The generalized SBM theory

In Eq. (4) $\hat{L}_\mathrm{S}$ is the Liouville super-operator governing the electron spin correlation function, which reads

$$\hat{L}_\mathrm{S}(\beta_\mathrm{LM}) = \hat{L}_0^{\mathrm{Zeeman}} + \hat{L}_0^{\mathrm{ZFS}}(\beta_\mathrm{LM}) + \mathrm{i}\hat{R}_{\mathrm{ZFS}}(\beta_\mathrm{LM}), \tag{9}$$

where the angular-dependent Liouville super operator $\hat{L}_\mathrm{S}(\beta_\mathrm{LM})$ is composed of a Zeeman term, a static ZFS term, and a Redfield super operator. The Zeeman Hamiltonian is

$$H_0^{\mathrm{Zeeman}} = -\hbar\gamma_\mathrm{S}B_0S_0^1, \tag{10}$$

where γ_S is $-1.76084\times10^{-11}\,\mathrm{rad\,s^{-1}}$. The static ZFS-interaction can be expressed in Hamiltonian form as

$$H_0^{\mathrm{ZFS}}(\beta_\mathrm{ML}) = \sqrt{\frac{2}{3}}D_\mathrm{s}S_\mathrm{PM}d_{00}^2(\beta_\mathrm{LM})S_0^2, \tag{11}$$

where we denote the principal component of the ZFS tensor D_s times the order parameter $\langle d_{00}^2(\beta_\mathrm{PM})\rangle \equiv S_\mathrm{PM}$, $D_\mathrm{s}S_\mathrm{PM}$, a ZFS parameter $\Delta_\mathrm{s}^{\mathrm{ZFS}}$, and S_0^2 is a standard second rank electron spin operator. $d_{00}^2(\beta_\mathrm{IJ})$ is a reduced Wigner rotation matrix element [61]. We may formulate the spin matrix $M_{\sigma\sigma}$ in Eq. (4) and invert it in order to obtain the relevant matrix elements in closed form. The details are presented in the Appendix A.

2.2.1. Dynamic models of the transient ZFS-interaction

Model I's electron spin spectral densities are angle-dependent because the reorientational motion is assumed very slow, which means the complex motion is in rigid limit and do not contribute to the electron spin relaxation times. The transient ZFS-interaction is described by an anisotropic pseudo-rotation diffusion model [6,62], which results in the following spectral densities:

$$J_n(n\omega_\mathrm{S}(m_\mathrm{I})) \equiv \frac{\Delta_\mathrm{t}^2}{5}\sum_k \left|d_{kn}^2(\beta_\mathrm{LM})\right|^2 \frac{\tau_k}{1+(n\omega_\mathrm{S}(m_\mathrm{I})\tau_k)^2} \tag{12}$$

with the dynamic frequency shift Q_n defined by

$$Q_n(n\omega_\mathrm{S}(m_\mathrm{I})) \equiv -\frac{\Delta_\mathrm{t}^2}{5}\sum_k \left|d_{kn}^2(\beta_\mathrm{LM})\right|^2 \frac{\tau_k^2 n\omega_\mathrm{S}(m_\mathrm{I})}{1+(n\omega_\mathrm{S}(m_\mathrm{I})\tau_k)^2}. \tag{13}$$

The correlation times are then given as

$$\frac{1}{\tau_0} = \frac{1}{\tau_\perp}, \tag{14}$$

$$\frac{1}{\tau_{\pm1}} = \frac{5}{6\tau_\perp} + \frac{1}{6\tau_\parallel}, \tag{15}$$

$$\frac{1}{\tau_{\pm2}} = \frac{1}{3\tau_\perp} + \frac{2}{3\tau_\parallel}, \tag{16}$$

where the dynamics reflect the symmetry breaking motions in the first coordination sphere of the paramagnetic ion. If only one water molecule is coordinated to Gd-ion and other coordinating atoms are from a ligand or from the macromolecule then the "fast" or "spinning" motion ($\tau_\parallel$) is expected to reflect the flickering/wagging motion of the water molecule because it is most flexible and is expected to be in the range of 1–5 ps. The flexibility of the complex due to the other coordinating atoms and ligands is expected to be slower and is thought influence the 'perpendicular' motion describe by $\tau_\perp$. This motion is expected to be approximately in the range: $\tau_\parallel < \tau_\perp < 100\,\mathrm{ps}$. A detail relation between correlation times and the transient ZFS-interaction is not possible to give unless a quantum chemical calculation is

preformed with real water. A simplified attempt to do such an analysis has been suggested, however the ligands in this case were not water molecules but spheres [59,60].

Model II simplifies the dynamic description of the transient ZFS assuming an isotropic pseudo rotational diffusion model, described by one correlation time τ_f. However, in addition we assume that the coordination sphere is *permanently disturbed* resulting in a static ZFS-interaction which is modulated by the rotational diffusion motion of the paramagnetic complex. This simple model was first suggested by Dwek [7] for biochemical systems. The electron spin spectral densities are given in this case by:

$$J_n(n\omega_s) = \frac{\Delta^2}{5}\frac{\tau_f}{1+(n\omega_s\tau_f)^2} + \frac{\Delta_s^2}{5}\frac{\tau_R}{1+(n\omega_s\tau_R)^2} \tag{17}$$

with the dynamic frequency shift Q_n defined by

$$Q_n(n\omega_s) = -\left(\frac{\Delta_t^2}{5}\frac{\tau_f^2 n\omega_s}{1+(n\omega_s\tau_f)^2} + \frac{\Delta_s^2}{5}\frac{\tau_R^2 n\omega_s}{1+(n\omega_s\tau_R)^2}\right), \tag{18}$$

where τ_f is the short correlation time of transient ZFS.

Eqs. 17 and 18 give the spectral densities of Model **II**, describing electron spin relaxation and the dynamic shift due to both local distortion within the first hydration shell and a reorientational modulation of a static ZFS. It is assumed that $\omega_s \approx (\omega_s \pm \Delta_s)$ which is valid in the high field limit. Thus, Eqs. 17 and 18 describe flexible (τ_f) low-symmetric Gd-complex attaches to slow (τ_R) tumbling macromolecules. However, the τ_R-modulated relaxation contribution vanishes for sufficient slow tumbling ($\tau_R\omega_s > 1$). If τ_R falls in the range $\Delta_s \cdot \tau_R > 1$, the perturbation condition which Eqs. 17 and 18 are based on is not fulfilled. The electron spin relaxation description then becomes a slow-motion problem which must be treated within the stochastic Liouville formalism. If $\Delta_s \cdot \tau_R < 1$ model **II** is valid also for "slow" tumbling macromolecules.

2.3. General trends of GSBM and SBM theories

Fig. 1 displays the relative difference between GSBM and SBM theory using the simplest spectral density model reading

$$J_n(n\omega_s) = \frac{\Delta^2}{5}\frac{\tau_f}{1+(n\omega_s\tau_f)^2} \tag{19}$$

and without static ZFS term. There is a marked discrepancy between SBM and GSBM at intermediate field strength. The multiexponential electron spin relaxation introduces differences which are at most 2%.

In the case of model **I** the relative difference between GSBM and SBM theory is also checked and displayed in Fig. 2. Increasing the static ZFS-interaction enlarges the difference between GSBM and SBM theory in the low-field region. Ignoring the static ZFS-interaction would lead to overestimated relaxation rates at low fields.

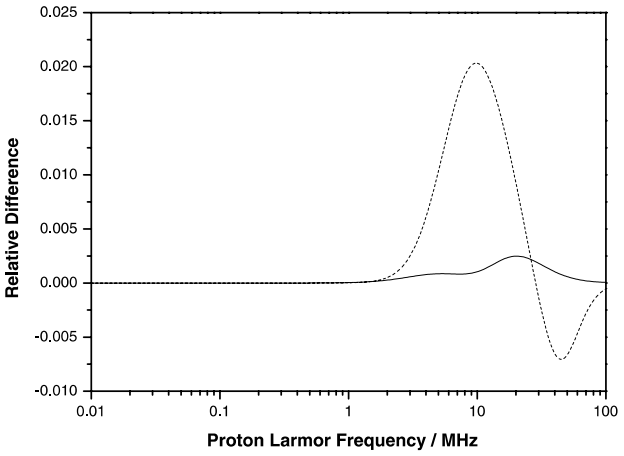

Fig. 1. The relative difference of GSBM and SBM theories are displayed as [GSBM-SBM]/SBM using the spectral density of Eq. (19). The parameters are the same as those used in model II NMRD fitting for Gd-DTPA (solid line) and MS-325+HSA (dash line) except that the static ZFS-interaction is 0.

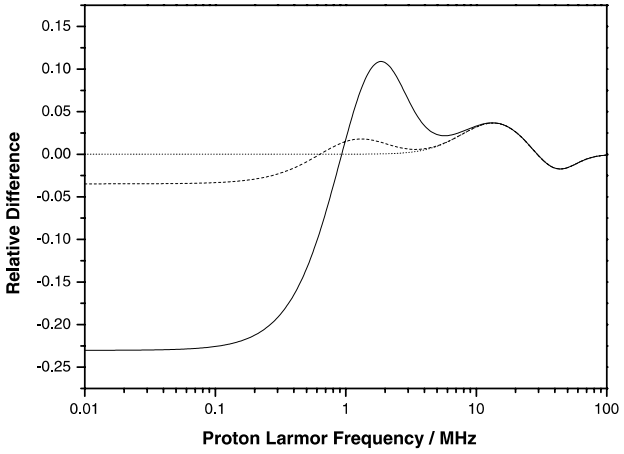

Fig. 2. The relative difference [GSBM-SBM]/SBM of GSBM and SBM theories is displayed for model **I**. The parameters are the same as those used in model **I** for the best T_1-NMRD profile of MS-325 + HSA, but the static ZFS-interactions are varied; 0.05 cm^{-1} (solid line), 0.01 cm^{-1} (dash line), and 0 cm^{-1} (dot line).

Figs. 3A–C display three sets of water proton T_1 NMRD-profiles corresponding to Gd-DTPA modified complexes. These calculated NMRD profiles applying GSBM theory on model **I** display the effects of reorientational correlation time τ_R and the size of the static ZFS-interaction Δ_s on the water proton relaxivity. In each panel 4 reorientational correlation time simulations are shown ranging from $\tau_R = 120$ ps to $\tau_R = 120$ ns. The effect of increasing static ZFS is shown from (A) through (C), where Δ_s increases from $\Delta_s = 0.1\ \Delta_t$ to $\Delta_s = 1\Delta_t$ to $\Delta_s = 10\ \Delta_t$, where the transient ZFS-interaction is fixed at $\Delta_t = 0.04\ cm^{-1}$.

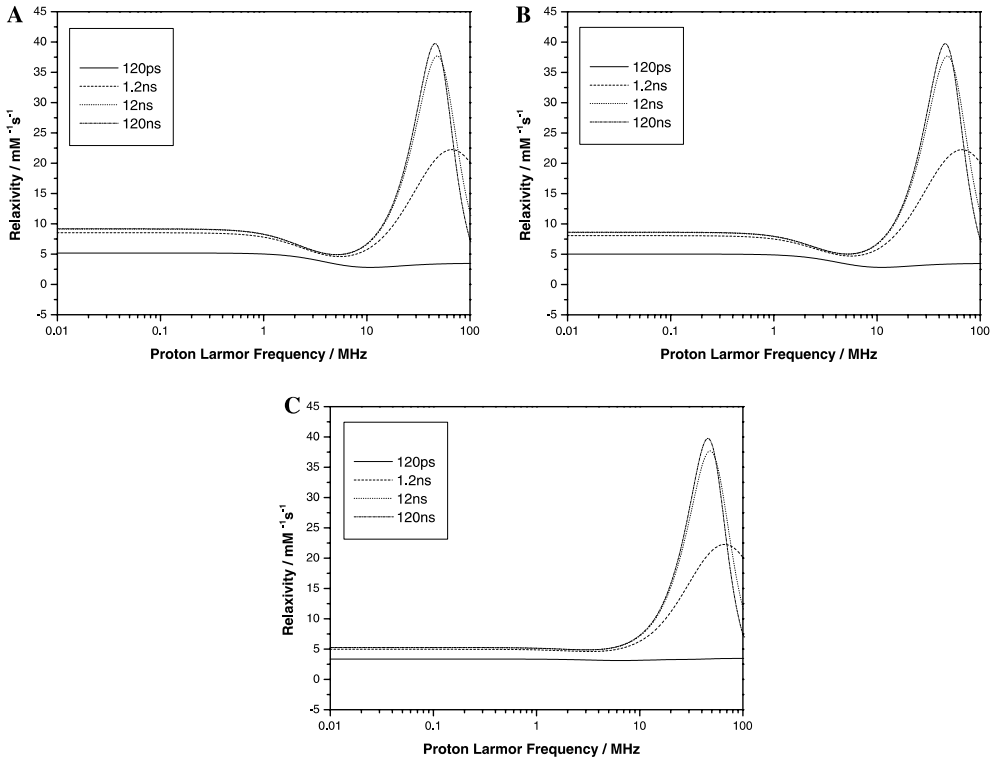

Fig. 3. T_1 NMRD profiles of Gd-DTPA from model **I** in the GSBM theory, which generally demonstrate the trend of proton relaxivity due to the change of static ZFS Δ_s and the rotational correlation time τ_R. $\Delta_s = 0.1\Delta_t$ in (A), $\Delta_s = \Delta_t$ in (B), and $\Delta_s = 10\Delta_t$ in (C), where $\Delta_t = 0.04\,cm^{-1}$.

MRI scanners have magnetic fields usually ranging from 0.1 T (4 MHz) to 3 T (125 MHz). The relevant part of the NMRD profiles in Fig. 3 is thus the proton frequencies above 4 MHz. One should remember that neither the GSBM theory nor the traditional SBM theory are valid in the low-field regime. Both GSBM and SBM are high field theories, valid only when the Zeeman interaction, is larger than the ZFS-interactions.

The trend of the GSBM (and SBM) theory is that there is an increase in the PRE effect, at high fields, because of a decrease in the electron spin–lattice relaxation rates. At high fields the reorientational time is the dominant correlation time. As τ_R becomes large, there is a second dispersion at higher fields as $\omega_I\tau_R > 1$, and the PRE effect begins to decrease. In the intermediate field region, 4–20 MHz the PRE behavior is much more complex because both electron spin–spin and spin–lattice relaxation rates are important for the water T_1-NMRD profiles.

Fig. 3B displays the NMRD profile of a modified Gd-DTPA complex with a much larger static ZFS-interaction parameter ($\Delta_s = \Delta_t$) than that of Fig. 3A ($\Delta_s = 0.1\Delta_t$). A small increase in relaxivity is noticed with increasing reorientational correlation times over the whole range of magnetic field strengths, but the largest PRE-effect is at high fields where the absolute value of the relaxivity reaches a maximum for largest τ_R. In absolute value the maximum relaxivity is the same in all Figs. 3A–C. Fig. 3C simulates a Gd-DTPA complex which is heavily distorted, thus characterized by a large static ZFS-interaction parameter ($\Delta_s = 10\Delta_t$). The relaxivity very clearly increases with the increase of the reorientational correlation time τ_R. Interestingly, the maximal relaxivity values at intermediate fields (4–10 MHz), are almost the same for all three static ZFS-interactions, thus independent of the distortion.

The philosophy of obtaining effective Gd-contrast agents thus becomes clear from these results. First, an increase of the reorientational correlation time of the contrast agent clearly increases the contrast effect at fields above 0.1 T. At intermediate fields, depending on the size of the static ZFS-interaction, the reorientational correlation time must take larger values in order to keep the relaxation enhancement effect on the same level. However, at higher fields where most clinical scanners operate (1.5 T), electron spin–lattice relaxation rates have become too long to influence relaxivity, and the most important parameter is the reorientational correlation time.

There is also another effect which may improve the relaxivity of a Gd-chelate bound at a macromolecule. One may expect a slightly more rigid Gd-chelate when it is attached to a macromolecular interface. This effect may decrease the transient ZFS-interaction which thus decreases the electron spin relaxation rates.

The general conclusion from these simulations is the same for both the SBM and GSBM approaches.

The differences appear in the magnitude of the microscopic parameters.

3. T_1 NMRD and ESR lineshape calculations

The gadolinium chelate MS-325 is displayed in Fig. 4. It is currently undergoing human clinical trials for imaging blood vessels. It has been reported to have good affinity for serum albumin; there is also a dramatic increase in proton relaxation enhancement in the presence of serum [63].

In this section we analyze the experimental water T_1-NMRD profile of a gadolinium chelate MS-325 together with the multifrequencies (X-, Q-, U-, and W-bands) ESR spectra. Relaxation rates and ESR spectra were measured either in the absence of human serum albumin (HSA), where the Gd(III) complex is expected to have a relatively short reorientational correlation time, or in the presence of HSA where the reorientational correlation time is expected to be much longer.

According to Eq. (12) the ESR lineshape function $I(\omega)$ of **model I** is a function of Δ_t^{ZFS}, Δ_s^{ZFS}, $\tau_\perp$, and $\tau_\parallel$, while $I(\omega)$ of **model II** (cf. Eq. (17)) is a function of Δ_t^{ZFS}, Δ_s^{ZFS}, τ_f, and τ_R. The amplitude of the proton T_1-NMRD profile is determined by the electron-nuclear dipole–dipole strength (cf Eq. (2)). Because of the decomposition approximation [6] there is a rotational diffusion modulation of the electron-nuclear dipole–dipole interaction which is independent of the rotational modulation of the electron spin relaxation. This is expected to be an accurate approximation because the electron spin relaxation time is not in the same timescale as the rotational diffusion of the complex.

3.1. Experimental description

The ^{1}H NMRD experiments were carried out using a field cycling relaxometer at New York Medical College [65]. T_1 relaxation rates for 1 mM MS-325 [63] in phosphate buffered saline, PBS, (10 mM NaPi, 150 mM NaCl, pH 7.4) or 0.1 mM MS-325 in 22.5% (w/v) human serum albumin, HSA, (Sigma, Fraction V Powder 96–99% albumin, containing fatty acids) were determined at 0.01, 0.03, 0.1, 0.3, 1, 2, 4, 6, 10, 15, 20, 30, 40, and 50 MHz at 35 °C. Relaxivities were determined using:

$$r1 = \left(1/T_1^{obs} - 1/T_1^{dia}\right)/[Gd], \tag{20}$$

where $1/T_1^{obs}$ is the observed relaxation rate and $1/T_1^{dia}$ is the relaxation rate of the diamagnetic medium with or without HSA. In the presence of HSA, most of the MS-325 is bound to the protein (95%) [63]. In order to estimate the relaxivity contribution from the inner-sphere water molecule of MS-325, the relaxivity of compound **1** (Fig. 4) was determined in the presence or absence of 22.5% HSA. Compound **1** is based on the acyclic amino acid ligand TTHA which is known to coordinate Gd without any inner-sphere water molecules [66]. Under these conditions compound **1** is about 99% bound to the protein [63]. Compound **1** is used as a surrogate for the relaxation enhancement arising from water molecules not in the inner-sphere of the Gd ion. The relaxation enhancement due to the inner-sphere water molecule of MS-325 was estimated by subtracting the relaxivity of **1** from the relaxivity of MS-325 (either in the presence of absence of HSA).

The ESR studies were performed with either 1 mM MS-325 in PBS or 0.1 mM MS-325 in 4.5% (w/v) HSA in PBS. The lower concentration of MS-325 was used in the protein study to ensure that most of the complex was protein bound under these conditions. All studies were performed at ambient temperature (20 °C). X-band studies were performed with a Varian E-112 spectrometer with a Varian TE_{102}. Solutions were drawn into a quartz flat cell. The Q-band measurements were obtained on a Varian E-115 spectrometer with a Varian TE_{011} cavity. Samples were placed in fused quartz capillaries. At U-band the sensitivity was insufficient to measure the 0.1 mM sample with HSA. U- and W-band

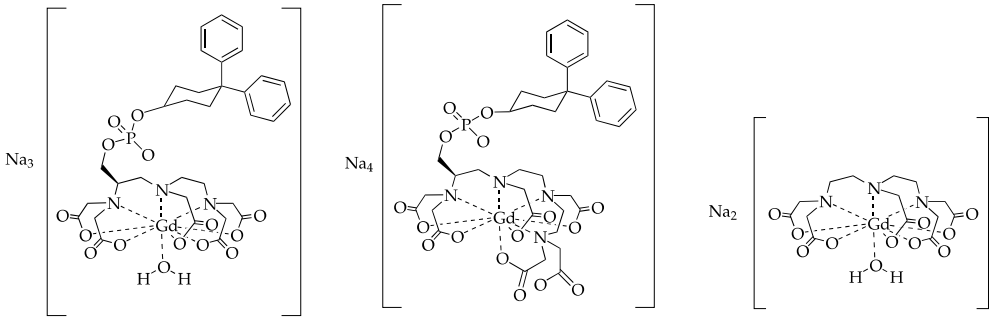

Fig. 4. The structure of MS-325, the $q = 0$ analogue compound **1** and Gd-DTPA.

studies were conducted on instruments built at the University of Illinois ESR Research Center [67,68].

The experimental NMRD data are the observed relaxivity, which is a sum effect of the inner-sphere water directly coordinating to the complex and all other outer-sphere water hydrating the complex in the 2nd and 3rd coordination spheres [63]. The NMRD data are displayed as relaxivity ($mM^{-1}s^{-1}$) vs Larmor frequency (MHz). Fig. 5 shows the observed relaxivity R_1^{obs} and outer-sphere relaxivity R_1^{out} as well as the inner-sphere relaxivity $R_1^{in} = R_1^{obs} - R_1^{out}$.

The ESR data are X-, Q-, and W-bands spectra of MS-325 with the presence of HSA, and Q-, U-, and W-bands spectra without HSA. The experimental ESR spectra are displayed in Fig. 6 with magnetic field in Gauss vs amplitude (a.u.). The X-band MS-325 + HSA differs from a smooth Lorenzian like signal whereas the corresponding W-band spectrum has impurities but displays a nice Lorenzian like signal. The theoretical ESR lineshapes reproduce line widths at all frequencies but a good fit to the lineshape is only accomplished at one frequency. This is a partly effect of the too simple dynamic models and different dynamic regimes influence the ESR spectra at different frequencies.

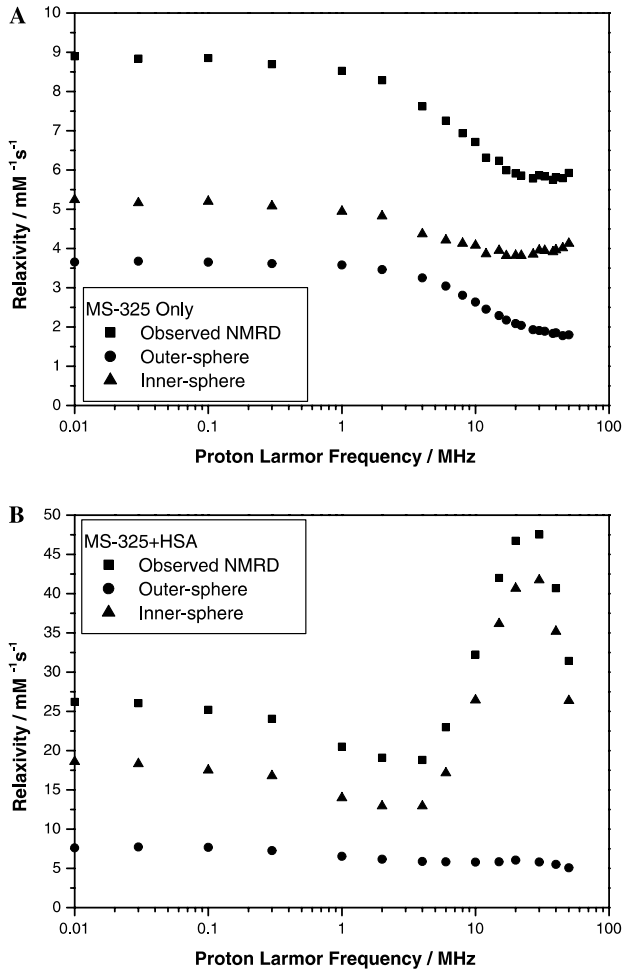

Fig. 5. Experimental water T_1-NMRD profiles of MS-325 with and without HSA.

3.2. Results and discussion

MS-325 is a derivative of Gd-DTPA complex, which is expected to have a longer reorientational correlation time. There have been two reports illustrating the effects of different microscopic parameters on the relaxivity of MS-325 [63,64], there have been no reports on the ESR lineshape of MS-325 to date.

This section presents a microscopic characterization of MS-325 and MS-325 + HSA based on NMRD profiles and ESR lineshape analyses. The ESR spectra are recorded at different magnetic fields ranging from X-, Q-, U-, and W-bands (include frequencies). The experimental ESR linewidths together with calculated ones are summarized in Table 1.

All model parameters resulting from NMRD fitting are summarized in Table 2 and from ESR lineshape fittings in Table 3. The Gd-aquo complex and Gd-DTPA fitting parameters are also included where the experimental NMRD curves and ESR linewidths used in the fitting are from [50–52]. We believe that the relative trends of model parameters are quite reliable whereas the absolute values are less accurate because they depend more on the dynamic model used. Parameters describing Gd-DTPA are modified slightly for MS-325 without HSA. It means that the chemical modification is changing the electron spin relaxation and the flexibility of the Gd(III) cavity and its symmetry.

The molecular weight of the paramagnetic complexes increase, ranging from the aquo-complex $[Gd(H_2O)_8]^{3+}$, Gd-DTPA, MS-325 to the heaviest complex MS-325 binding to HSA. Consequently, the rotational correlation time increases with the molecular weight and a marked increase in τ_R is expected for MS-325 binding to HSA.

3.2.1. MS-325

The NMRD profile of MS-325 is rather featureless. It could be reproduced using the parameters listed for models **I** and **II** in Table 2. Since MS-325 is slightly modified compared to Gd-DTPA, but with the same coordination environment and number of waters coordinated (q), we also re-analyzed the NMRD profile of Gd-DTPA with our models. Perhaps not surprisingly, the transient ZFS-interaction is the same as for MS-325 as for Gd-DTPA ($\Delta_t = 0.04\,cm^{-1}$). The reorientational correlation time of MS-325 increases to 100 ps compared with 70 ps of Gd-DTPA. According to analysis based on the SBM theory the reorientational correlation time is 115 ps [63]. The theoretical NMRD profiles are shown in Fig. 7 and conform well to the experimental profile. Other parameters are the same as in other work.

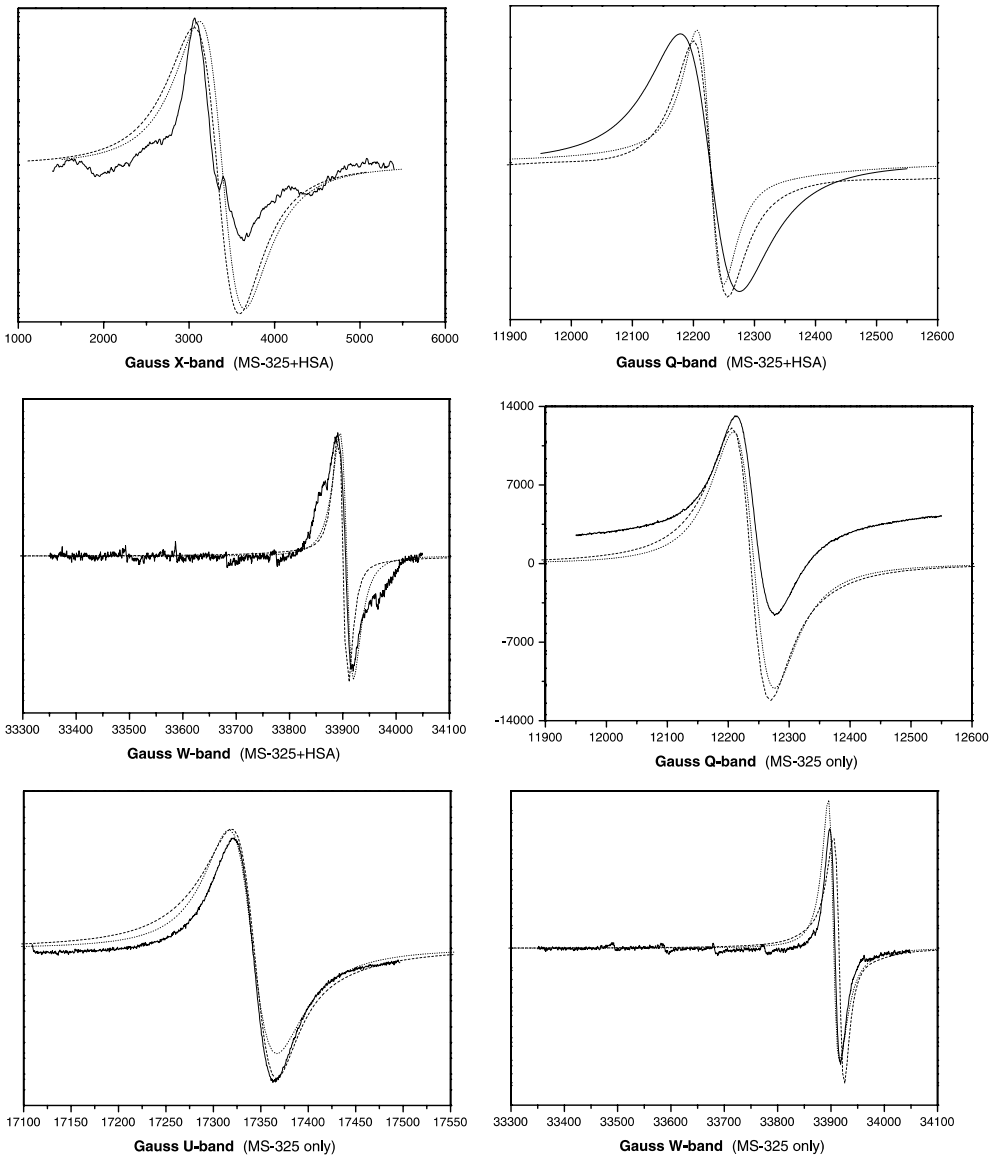

Fig. 6. The ESR spectra in the experiments (solid line), Model **I** (dash line) and Model **II** (dot line). In the experiments, Q- and W-bands have spectra both with and without albumin. It is observed that: (1) there is a frequency offset between the bound (with albumin) and unbound spectra that decreases as the field increases; (2) the spectra in the presence of albumin is broader than in the absence of albumin. The small peaks in the W-band spectra arise from a Mn(II) impurity in the cavity.

Table 1
Experimental and calculated linewidths of ESR lineshapes expressed as exp./model **I**/model **II** in Gauss (G)

Gd Complex	X-band (G)	Q-band (G)	U-band (G)	W-band (G)
MS-325	580/536/500	62/64/72	41/32/36	19/12/12
MS-325 + HSA	550/524/500	97/56/44	—/32/24	28/12/6

The experimental ESR linewidths of W-, U-, and Q-bands at 293 K are 19, 41, 62, and 580 G, respectively. They are listed in Table 1 and should be compared with the linewidth of our simulations at 310 K. For model **I** we obtained 12, 32, 64, and 536 G, and in model **II** 12, 36, 72, and 500 G at W-, U-, Q-, amd X-bands.

3.2.2. MS-325 + HSA

The NMRD profile for MS-325 + HSA is shown in Fig. 8 along with the best fits for models **I** and **II**. In this case the NMRD profile indicates a drastic change in the flexibility of the Gd environment. The transient ZFS-interaction drops from $0.04\,cm^{-1}$ for MS-325 to

Table 2
Parameters for Gd complexes in NMRD fitting

Gd Complex	Fig./model	Δ_t (cm^{-1})	Δ_s (cm^{-1})	$\tau_\perp,\tau_\parallel/\tau_f$ (ps)	τ_R (ps)	r_{IS} (Å)	q	τ_M (ns)
$[Gd(H_2O)_8]^{3+}$	(I)	0.04	0.01	10, 25	40	3.13	8	2
	(II)	0.04	0.01	10	40	3.13	8	2
	[a]	0.05	—	6	32	3.00	8	—
Gd-DTPA	(I)	0.04	0.01	12, 25	70	3.13	1	126
	(II)	0.04	0.01	12	70	3.13	1	126
	[a]	0.0585	—	6	45	3.10	3	—
MS-325	(I)	0.04	0.15	18, 25	100	2.95	1	72
	(II)	0.04	0.011	18	100	2.95	1	72
	[b]	NA	—	NA	115	3.10	1	69
MS-325 + HSA	(I)	0.017	0.05	26, 20	10,000	3.13	1	198
	(II)	0.018	0	30	10,000	3.13	1	198
	[b]	0.015	—	21	13,300	3.10	1	170

NA, not available.
[a] Ref. [53].
[b] Ref. [63] (310 K).

Table 3
Parameters for Gd complexes in ESR fitting

Gd Complex	Fig./model	Δ_t (cm^{-1})	Δ_s (cm^{-1})	$\tau_\perp,\tau_\parallel/\tau_f$ (ps)	τ_R (ps)
$[Gd(H_2O)_8]^{3+}$	(I)	0.04	0.01	10, 25	—
	(II)	0.04	0.01	10	40
	[a]	0.05	—	6	32
Gd-DTPA	(I)	0.04	0.01	12, 25	—
	(II)	0.04	0.01	12	70
	[a]	0.0585	—	6	45
MS-325	(I)	0.04	0.15	18, 25	—
	(II)	0.04	0.011	18	100
	No Ref.				
MS-325 + HSA	(I)	0.04	0.05	26 ,20	—
	(II)	0.04	0.001	30	10,000
	No Ref.				

[a] Ref. [53].

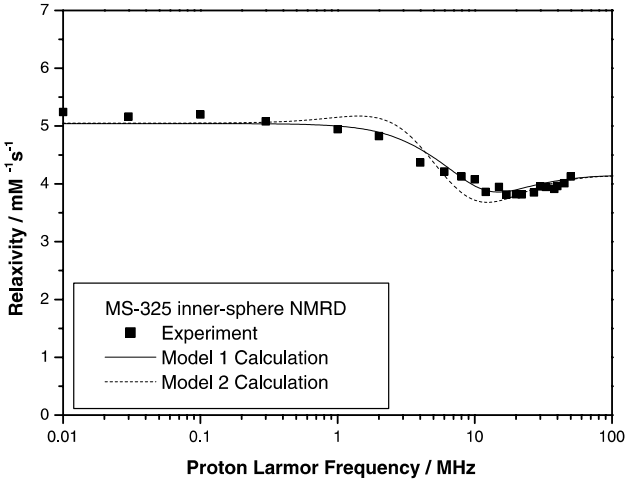

Fig. 7. The best fit of the inner-sphere contribution to the water T_1-NMRD profile of MS-325 complex at $T = 310$ K. Parameters of models **I** and **II** are listed in Table 2.

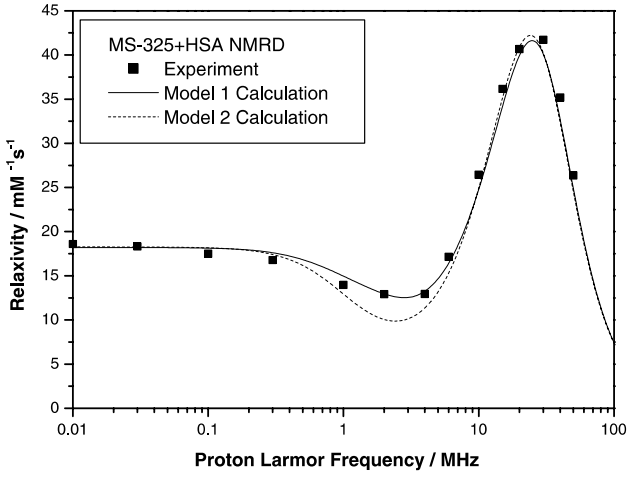

Fig. 8. The best fit of the inner-sphere contribution to the water T_1-NMRD profile of the Gd(III) MS-325 + HSA complex at $T = 310$ K. Model parameters are listed in Table 2.

$0.017\,cm^{-1}$ for MS-325 + HSA. In this analysis the same parameters of $\tau_R, r_{IS}, q, \tau_M$ are used as have been extracted using the SBM theory [63].

However, the ESR parameters of the NMRD fitting differ from those obtained from the ESR fitting. If the transient ZFS-interaction obtained from the MS-325 + HSA NMRD fitting is used, the ESR linewidths are underestimated. In addition, the experimental ESR lineshape at X-band is not symmetric and seems to indicate other effects perhaps of slow-motion origin upon binding. If we recalculated the ESR X-band spectra by focusing only on the left-hand rather narrow part of the spectra it may be well reproduced using $\Delta_t = 0.025\,cm^{-1}$, which is similar to the best fit value obtained from the NMRD profile.

The peaks of the NMRD profiles in Fig. 8 are around 30 MHz. If we use the larger $\Delta_t = 0.04\,cm^{-1}$ value which better reproduces the experimental ESR-linewidth, there is a marked shift of the NMRD peak to higher field, which is shown in Fig. 9.

The rotational correlation time τ_R of MS-325 is dramatically changed upon binding to HSA. This results in a marked increase in relaxivity compared to MS-325 without HSA. In addition it appears that the transient ZFS-interaction is decreased when MS-325 associates with HSA. This result thus indicates a more rigid character of the MS-325 + HSA complex which is not observed for MS-325 without HSA or Gd-DTPA.

The experimental ESR linewidth of MS-325 with HSA at W-, Q-, and X-bands are 28, 97, and 550 G at 293 K (see Table 1). There is no U-band experimental data for MS-325 + HSA. The linewidth from our calculation at 310 K are 12, 32, 56, and 524 G in model **I** and for model **II** are 6, 24, 44, and 500 G, at W-, U-, Q-, and X-bands, respectively.

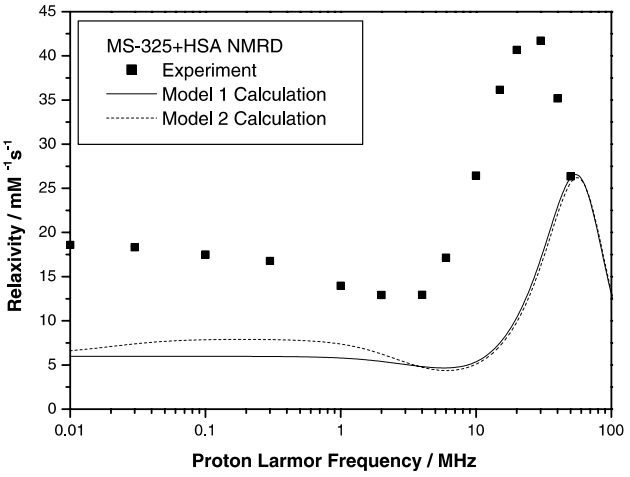

Fig. 9. The best fit of the inner-sphere contribution to the water T_1-NMRD profile of MS-325 + HSA complex at $T = 310\,K$ using the ESR parameters in Table 3 together with other parameters in Table 2. As we can see here the maximum relaxivity occurs at around 50 MHz which is not consistent with experiment.

3.3. Conclusions

Although parameters of NMRD and ESR fitting are consistent for Gd-aquo complex, Gd-DTPA, and MS-325, a problem in the analysis arises when the MS-325 associates with HSA. There is a drastic increase in the rotational correlation time and a marked decrease in Δ_t upon binding. The latter effect is derived from analysing the experimental NMRD profile which shows a maximum relaxivity at a proton Larmor frequency of about 30 MHz. This marked increase of relaxivity is due to a decrease in the electron spin–lattice relaxation rates, coupled with the long reorientational correlation time. In Fig. 9 the inconsistence between the NMRD $\Delta_t = 0.017\,cm^{-1}$ and ESR parameter value $\Delta_t = 0.04\,cm^{-1}$ is shown. The simulated NMRD profile with $\Delta_t = 0.04\,cm^{-1}$ shows a maximum at 50 MHz. A reasonable explanation for the discrepancy between the NMRD and ESR fittings of MS-325 + HSA complex is because the electron spin–spin relaxation time is sensitive for slow motions whereas the T_1-NMRD profile is dominated by the electron spin–lattice relaxations rates where slow motions are less important. The dynamic model **I** does not include such slow modulation of the ZFS-interaction and thus the ESR linewidth has to be reproduced using fast dynamics and a larger transient ZFS-interaction. The latter is thus overestimated in order to reproduce the ESR linewidth. This discrepancy may call for a more detail analysis of the X-band ESR spectra of MS-325 + HSA.

Our NMRD analysis suggests that MS-325 becomes more rigid when bound to HSA. This effect is manifested in a marked decrease in the transient ZFS-interaction parameter. Combining this effect with the long reorientational time explains the increase of relaxivity relative to MS-325 without HSA. It was also observed that multiexponentiallity of electron spin relaxation and dynamic shifts introduced a discrepancy between GSBM and SBM which is less than 2.0% in the intermediate field strength(1–10 MHZ) and for the best fitting parameters describing MS-325 + HSA it is about 10% (Fig. 2). The SBM picture and the GSBM picture predict the same trends but differ in the microscopic parameters describing the electron spin relaxation rates. The local fluctuation τ_f of the Gd-ion is very much the same for all complexes analyzed.

The magnetic fields relevant for MRI are usually between 0.1 and 3 T. In this field interval the magnitude of the Zeeman energy of the Gd(III) ion ranging between 0.1–3 cm^{-1} which is large compared with the ZFS-interaction in our calculations. The conditions of the high field GSBM theory are thus fulfilled.

4. Summary

This work developed a generalized SBM theory for low-symmetry Gd($S = 7/2$) complexes which describing

water T_1-NMRD profiles and ESR lineshapes. The differences between SBM and GSBM because of multi-exponential electron spin relaxation and static ZFS-interaction are clearly shown.

The Gd(III) complex MS-325 is electronically quite similar to Gd-DTPA. Differences in relaxivity arise from the increased reorientational time of the larger MS-325 complex. In the presence of HSA, the whole complex(MS-325 + HSA) has a considerably increased reorientational correlation time τ_R and an increased rigidity of the Gd-ion environment(a decreased Δ_t). Consequently, the electron spin–lattice relaxation rates decrease and the NMR relaxation rate of water increases relative to MS-325 without HSA.

The ESR X-band lineshape of MS-325 + HSA is complex and only partly supports this conclusion because its shape is not yet completely understood.

Appendix A. The electron spin–spin spectral density

The redfield matrix describing electron spin–spin relaxation for $S = 7/2$ can be represented in Zeeman basis, and if rewrite it with symbols, then we have:

$$\mathbf{R} = \begin{bmatrix} A & B & C & 0 & 0 & 0 & 0 \\ B & D & E & F & 0 & 0 & 0 \\ C & E & G & 0 & H & 0 & 0 \\ 0 & F & 0 & I & 0 & F & 0 \\ 0 & 0 & H & 0 & G & E & C \\ 0 & 0 & 0 & F & E & D & B \\ 0 & 0 & 0 & 0 & C & B & A \end{bmatrix}, \tag{A.1}$$

where the matrix elements are given in the following Table.

Matrix elements of $R(\beta_{LM})$ for $S = 7/2$

$A = 54J_0 + 174J_1 + 66J_2 - i78Q_1 + i24Q_2$
$B = -24\sqrt{21}J_1$
$C = -6\sqrt{105}J_2$
$D = 24J_0 + 174J_1 + 126J_2 - i18Q_1 - i6Q_2$
$E = -24\sqrt{5}J_1$
$F = -60\sqrt{3}J_2$
$G = 6J_0 + 78J_1 + 186J_2 + i18Q_1 - i24Q_2$
$H = -120J_2$
$I = 30J_1 + 210J_2 + i30Q_1 - i30Q_2$

Then we add the static ZFS-interaction term, defined as

$$\hat{H}_0^{ZFS}(\beta_{LM}) = \sqrt{\frac{2}{3}} D_s S_{PM} d_{00}^2(\beta_{LM}) \hat{S}_0^2, \tag{A.2}$$

where S_{PM} is an order parameter given by $S_{PM} = \langle d_{00}^2(\beta_{PM}) \rangle$. The resulting matrix is then transformed to an irreducible spherical electron spin tensor base with the operator basis set $\hat{O}_\sigma^\Sigma$

$$\hat{O}_\sigma^\Sigma = \sum_m \sqrt{2\Sigma + 1} \begin{pmatrix} S & S & \Sigma \\ m+\sigma & -m & -\sigma \end{pmatrix} (-1)^{S-m-\sigma} \; | Sm+\sigma \rangle \langle Sm | \tag{A.3}$$

expressed in terms of Zeeman eigenoperators $| Sm+\sigma \rangle \langle Sm |$ and where

$$\begin{pmatrix} S & S & \Sigma \\ m+\sigma & -m & -\sigma \end{pmatrix} \tag{A.4}$$

is a 3j-symbol (ref. Brink-Satchler).

The resulting matrix is written with first even rank tensors and then odd rank tensors, in the order 2,4,6,1,3,5,7. The Zeeman matrix $\mathbf{1}i(\omega_I \pm \omega_S)$ is then added. We get a matrix of the form

$$\mathbf{M}_{\pm\mathbf{1}} = \begin{bmatrix} a & b & 0 & c & d & 0 & 0 \\ b & e & f & 0 & g & h & 0 \\ 0 & f & i & 0 & 0 & j & k \\ c & 0 & 0 & l & m & 0 & 0 \\ d & g & 0 & m & n & p & 0 \\ 0 & h & j & 0 & p & q & r \\ 0 & 0 & k & 0 & 0 & r & s \end{bmatrix} \tag{A.5}$$

with the elements defined in the following Table.

Matrix elements of $M_{\pm1}(\beta_{LM})$ for $S = 7/2$

$a = \frac{6}{7}(43J_0 + 51J_1 + 102J_2 - i51Q_1 + i8Q_2) + i(\omega_I \pm \omega_S)$
$b = \frac{12\sqrt{110}}{7}(J_0 + 2J_1 - 3J_2 - i2Q_1 + iQ_2)$
$c = 2\sqrt{3}D_s S_{PM} d_{00}^2(\beta_{LM})$
$d = 2\sqrt{\frac{22}{7}}D_s S_{PM} d_{00}^2(\beta_{LM})$
$e = \frac{6}{77}(402J_0 + 2281J_1 + 2707J_2 - i419Q_1 + i17Q_2) + i(\omega_I \pm \omega_S)$
$f = \frac{42\sqrt{10}}{11}(J_0 + 8J_1 - 9J_2 - i2Q_1 + iQ_2)$
$g = 4\sqrt{\frac{5}{7}}D_s S_{PM} d_{00}^2(\beta_{LM})$
$h = 2\sqrt{\frac{26}{11}}D_s S_{PM} d_{00}^2(\beta_{LM})$
$i = \frac{6}{11}(29J_0 + 375J_1 + 366J_2 - i3Q_1 - i26Q_2) + i(\omega_I \pm \omega_S)$
$j = 14\sqrt{\frac{5}{143}}D_s S_{PM} d_{00}^2(\beta_{LM})$
$k = 4\sqrt{\frac{3}{13}}D_s S_{PM} d_{00}^2(\beta_{LM})$
$l = 6(3J_0 + 5J_1 + 2J_2 - iQ_1 - i2Q_2) + i(\omega_I \pm \omega_S)$
$m = 6\sqrt{\frac{66}{7}}(J_0 - J_2 - i2Q_1 + iQ_2)$
$n = 2(18J_0 + 55J_1 + 77J_2 - i21Q_1 + i3Q_2) + i(\omega_I \pm \omega_S)$
$p = 4\sqrt{\frac{130}{77}}(3J_0 + 14J_1 - 17J_2 - i6Q_1 + i3Q_2)$
$q = \frac{2}{13}(159J_0 + 1427J_1 + 1534J_2 - i123Q_1 - i36Q_2) + i(\omega_I \pm \omega_S)$
$r = \frac{84}{143}\sqrt{165}(J_0 + 12J_1 - 13J_2 - i2Q_1 + iQ_2)$
$s = \frac{6}{13}(12J_0 + 209J_1 + 143J_2 + i41Q_1 - i53Q_2) + i(\omega_I \pm \omega_S)$

The element we are interested in is the [4,4] element of the inverted matrix of $M_{\pm 1}$.

Appendix B. The electron spin–lattice spectral density

Again we start with the Redfield matrix describing electron spin–lattice relaxation. The Zeeman basis is given in symbolic form

$$\mathbf{R} = \begin{bmatrix} A & B & C & 0 & 0 & 0 & 0 & 0 \\ B & D & E & F & 0 & 0 & 0 & 0 \\ C & E & G & H & I & 0 & 0 & 0 \\ 0 & F & H & J & 0 & I & 0 & 0 \\ 0 & 0 & I & 0 & J & H & F & 0 \\ 0 & 0 & 0 & I & H & G & E & C \\ 0 & 0 & 0 & 0 & F & E & D & B \\ 0 & 0 & 0 & 0 & 0 & C & B & A \end{bmatrix}, \tag{B.1}$$

where the matrix elements are given in the following Table.

Matrix elements of $R(\beta_{\mathrm{LM}})$ for $S = 7/2$

$A = 126J_1 + 42J_2$
$B = -126J_1$
$C = -42J_2$
$D = 222J_1 + 90J_2$
$E = -96J_1$
$F = -90J_2$
$G = 126J_1 + 162J_2$
$H = -30J_1$
$I = -120J_2$
$J = 30J_1 + 210J_2$

Then we transform the basis using the similar method as previous part. In this case the static ZFS-interaction term is zero. The transformed matrix has the following form

$$\mathbf{N} = \begin{bmatrix} 0 & 0 & 0 & 0 & 0 & 0 & 0 & 0 \\ 0 & A & 0 & H & 0 & 0 & 0 & 0 \\ 0 & 0 & B & 0 & I & 0 & 0 & 0 \\ 0 & H & 0 & C & 0 & J & 0 & 0 \\ 0 & 0 & I & 0 & D & 0 & K & 0 \\ 0 & 0 & 0 & J & 0 & E & 0 & L \\ 0 & 0 & 0 & 0 & K & 0 & F & 0 \\ 0 & 0 & 0 & 0 & 0 & L & 0 & G \end{bmatrix}, \tag{B.2}$$

The above matrix can be reduced to a 4×4 matrix since only odd-rank tensor operators enter the theoretical description. The final M_0 matrix is formed as

$$\mathbf{M_0} = \begin{bmatrix} a & e & 0 & 0 \\ e & b & f & 0 \\ 0 & f & c & g \\ 0 & 0 & g & d \end{bmatrix}, \tag{B.3}$$

where the matrix elements are given in the following Table.

Matrix elements of $M_1(\beta_{\mathrm{LM}})$ for $S = 7/2$

$a = 12(J_1 + 4J_2) - \mathrm{i}\omega_{\mathrm{I}} + \frac{1}{\tau_{\mathrm{R}}}$
$b = 12(12J_1 + 13J_2) - \mathrm{i}\omega_{\mathrm{I}} + \frac{1}{\tau_{\mathrm{R}}}$
$c = \frac{60}{13}(53J_1 + 51J_2) - \mathrm{i}\omega_{\mathrm{I}} + \frac{1}{\tau_{\mathrm{R}}}$
$d = \frac{168}{13}(8J_1 + 5J_2) - \mathrm{i}\omega_{\mathrm{I}} + \frac{1}{\tau_{\mathrm{R}}}$
$e = 24\sqrt{\frac{11}{7}}(J_1 - J_2)$
$f = 240\sqrt{\frac{13}{77}}(J_1 - J_2)$
$g = \frac{240}{13}\sqrt{\frac{343}{11}}(J_1 - J_2)$

The inverted matrix element is given by

$$tr_{\mathrm{S}}\left\{\hat{O}_0^{1\dagger}\widehat{M^{-1}}\hat{O}_0^1\right\} = \frac{bcd - df^2 - bg^2}{abcd - cde^2 - adf^2 - abg^2 + e^2g^2}. \tag{B.4}$$

Appendix C. The ESR lineshape function

The derivation of ESR lineshape function has the same procedure as that in the part of electron spin–spin spectral density. The differences are the definition of the **M** matrix and $\sigma = 1$. The matrix elements are given in the following Table.

ESR lineshape matrix elements, $\sigma = 1$

$a = \frac{6}{7}(43J_0 + 51J_1 + 102J_2 - \mathrm{i}51Q_1 + \mathrm{i}8Q_2) + \mathrm{i}(\omega + \omega_{\mathrm{S}})$
$b = \frac{12\sqrt{110}}{7}(J_0 + 2J_1 - 3J_2 - \mathrm{i}2Q_1 + \mathrm{i}Q_2)$
$c = 2\sqrt{3}D_{\mathrm{s}}S_{\mathrm{PM}}d^2_{00}(\beta_{\mathrm{LM}})$
$d = 2\sqrt{\frac{22}{7}}D_{\mathrm{s}}S_{\mathrm{PM}}d^2_{00}(\beta_{\mathrm{LM}})$
$e = \frac{6}{77}(402J_0 + 2281J_1 + 2707J_2 - \mathrm{i}419Q_1 + \mathrm{i}17Q_2) + \mathrm{i}(\omega + \omega_{\mathrm{S}})$
$f = \frac{42\sqrt{10}}{11}(J_0 + 8J_1 - 9J_2 - \mathrm{i}2Q_1 + \mathrm{i}Q_2)$
$g = 4\sqrt{\frac{5}{7}}D_{\mathrm{s}}S_{\mathrm{PM}}d^2_{00}(\beta_{\mathrm{LM}})$
$h = 2\sqrt{\frac{26}{11}}D_{\mathrm{s}}S_{\mathrm{PM}}d^2_{00}(\beta_{\mathrm{LM}})$
$i = \frac{6}{11}(29J_0 + 375J_1 + 366J_2 - \mathrm{i}3Q_1 - \mathrm{i}26Q_2) + \mathrm{i}(\omega + \omega_{\mathrm{S}})$
$j = 14\sqrt{\frac{5}{143}}D_{\mathrm{s}}S_{\mathrm{PM}}d^2_{00}(\beta_{\mathrm{LM}})$
$k = 4\sqrt{\frac{3}{13}}D_{\mathrm{s}}S_{\mathrm{PM}}d^2_{00}(\beta_{\mathrm{LM}})$
$l = 6(3J_0 + 5J_1 + 2J_2 - \mathrm{i}Q_1 - \mathrm{i}2Q_2) + \mathrm{i}(\omega + \omega_{\mathrm{S}})$
$m = 6\sqrt{\frac{66}{7}}(J_0 - J_2 - \mathrm{i}2Q_1 + \mathrm{i}Q_2)$
$n = 2(18J_0 + 55J_1 + 77J_2 - \mathrm{i}21Q_1 + \mathrm{i}3Q_2) + \mathrm{i}(\omega + \omega_{\mathrm{S}})$
$p = 4\sqrt{\frac{130}{77}}(3J_0 + 14J_1 - 17J_2 - \mathrm{i}6Q_1 + \mathrm{i}3Q_2)$
$q = \frac{2}{13}(159J_0 + 1427J_1 + 1534J_2 - \mathrm{i}123Q_1 - \mathrm{i}36Q_2) + \mathrm{i}(\omega + \omega_{\mathrm{S}})$
$r = \frac{84}{143}\sqrt{165}(J_0 + 12J_1 - 13J_2 - \mathrm{i}2Q_1 + \mathrm{i}Q_2)$
$s = \frac{6}{13}(12J_0 + 209J_1 + 143J_2 + \mathrm{i}41Q_1 - \mathrm{i}53Q_2) + \mathrm{i}(\omega + \omega_{\mathrm{S}})$

References

[1] A. Carrington, A.D. McLachlan, Introduction to Magnetic Resonance, A Harper Int. Ed, 1967, 1969.
[2] P. Caravan, J.J. Ellison, T.J. McMurry, R.B. Lauffer, Chem. Rev. 99 (1999) 2293.
[3] N. Bloembergen, J. Chem. Phys. 27 (1957) 572;
N. Bloembergen, J. Chem. Phys. 27 (1957) 595.
[4] N. Bloembergen, L.O. Morgan, J. Chem. Phys. 34 (1961) 842.
[5] J. Kowalewski, L. Nordenskiöld, N. Benetis, P.-O. Westlund, Prog. NMR Spectroc. 17 (1985) 141.
[6] P.-O. Westlund. in: J.J. Delpuech (Ed.), Ch. 4 in Dynamics of Solutions and Fluid Mixtures by NMR, Wiley, New York, 1995.
[7] R.A. Dwek, NMR in Biochemistry: Applications to Enzyme System, Clarendon Press, Oxford, 1973.
[8] D.E. Burton, S. Forsen, G. Karlström, R.A. Dwek, Progr. NMR Spectrosc. 13 (1979) 1–45.
[9] N. Benetis, L. Nordenskiöld, J. Kowalewski, H. Wennerström, P.-O. Westlund, Mol. Phys. 48 (1983) 329.
[10] N. Benetis, L. Nordenskiöld, J. Kowalewski, H. Wennerström, P.-O. Westlund, Mol. Phys. 50 (1983) 515.
[11] N. Benetis, L. Nordenskiöld, J. Kowalewski, H. Wennerström, P.-O. Westlund, J. Magn. Reson. 58 (1984) 261.
[12] P.-O. Westlund, H. Wennerström, L. Nordenskiöld, J. Kowalewski, N. Benetis, J. Magn. Reson. 59 (1984) 91.
[13] N. Benetis, L. Nordenskiöld, J. Kowalewski, H. Wennerström, P.-O. Westlund, Mol. Phys. 58 (1984) 282.
[14] I. Bertini, F. Briganti, C. Luchinat, M. Mancini, G. Spina, J. Magn. Reson. 59 (1984) 41.
[15] I. Bertini, C. Luchinat, M. Mancini, G. Spina, J. Magn. Reson. 59 (1984) 213.
[16] L. Banci, I. Bertini, F. Briganti, C. Luchinat, J. Magn. Reson. 66 (1986) 58.
[17] I. Bertini, C. Luchinat, NMR of Paramagntic Molecules in Biological Systems, Benjamin/Cummings, Menlo Park, California 1986.
[18] I. Bertini, C. Luchinat, K. Vasavada, J. Magn. Reson. 89 (1990) 243.
[19] L. Banci, I. Bertini, C. Luchinat, Nuclear and Electron Relaxation, VHC, Weinheim, 1991.
[20] I. Bertini, O. Galas, C. Luchinat, G. Parigi, J. Magn. Reson. 113 (1995) 151.
[21] S.H. Koneig, C. Baglin, R.D. Brown III, C.F. Brewer, Magn. Reson. Med. 1 (1984) 496.
[22] T. Bayburt, R.R. Sharp, J. Chem. Phys. 92 (1990) 5892.
[23] R.R. Sharp, J. Chem. Phys. 93 (1990) 6921.
[24] R. Sharp, J. Magn. Reson. 100 (1992) 491.
[25] R. Sharp, J. Chem. Phys. 98 (1993) 912.
[26] R. Sharp, J. Chem. Phys. 98 (1993) 2507.
[27] R. Sharp, J. Chem. Phys. 98 (1993) 6092.
[28] J. Bovet, R. Sharp, J. Chem. Phys. 99 (1993) 18.
[29] T. Bayburt, R.R. Sharp, J. Phys. Chem. 97 (1993) 4558.
[30] S.M. Abernathy, R. Sharp, J. Phys. Chem. A101 (1997) 3692.
[31] S.M. Abernathy, R. Sharp, J. Chem. Phys. 106 (1997) 9032.
[32] R. Sharp, S.M. Abernathy, L.L. Lohr, J. Chem. Phys. 107 (1997) 7620.
[33] S.M. Abernathy, J.C. Miller, L.L. Lohr, R. Sharp, J. Chem. Phys. 109 (1998) 4035.
[34] J.C. Miller, S.M. Abernathy, R. Sharp, J. Phys. Chem. A 104 (2000) 4839.
[35] J.C. Miller, R. Sharp, J. Phys. Chem. A 104 (2000) 4889.
[36] J.C. Miller, S.M. Abernathy, L.L. Lohr, R. Sharp, J. Phys. Chem. A 104 (2000) 9481.
[37] J.C. Miller, L.L. Lohr, R. Sharp, J. Magn. Reson. 148 (2001) 267.
[38] R. Sharp, L.L. Lohr, J.C. Miller, Progr. NMR Spectrosc. 38 (2001) 115.
[39] S. Rast, A. Borel, L. Helm, E. Belorizky, P.H. Fries, A.E. Merbach, J. Am. Chem. Soc. 123 (2001) 2637.
[40] S. Rast, P.H. Fries, E. Belorizky, J. Chem. Phys. 113 (2000) 8724.
[41] A. Borel, F. Yerly, L. Helm, A.E. Merbach, J. Am. Chem. Soc. 124 (2002) 2042.
[42] I. Bertini, J. Kowalwski, C. Luchnat, T. Nilsson, G. Parigi, J. Chem. Phys. 11 (1999) 5795.
[43] T. Nilsson, G. Parigi, J. Kowalewski, J. Phys. Chem. 106 (2002) 4476.
[44] D. Kruk, J. Kowalewski, J. Magn. Reson. 162 (2003) 229.
[45] D. Kruk, T. Nilsson, J. Kowalewski, Phys. Chem. Chem. Phys. 3 (2001) 4907.
[46] D. Kruk, J. Kowalewski, J. Biol. Inorg. Chem. 8 (2003) 512.
[47] J. Kowalewski, D. Kruk, G. Parigi, Advances in inorganic Chemistry. in: I. Bertini, R. van Eldik, (Eds.), vol. 57, Thematic issue on 'Relaxometry of water-metal ion interactions', 2003.
[48] M. Rubenstein, A. Baram, Z. Luz, Mol. Phys. 20 (1971) 67.
[49] P.-O. Westlund, Mol. Phys. 85 (1995) 1165.
[50] G. Hernandez, M.F. Tweedle, R.G. Bryant, Inorg. Chem. 29 (1990) 5109.
[51] S.H. Koenig, M. Epstein, J. Chem. Phys. 63 (1975) 2279.
[52] C.F.G.C. Geraldes, R.D. Brown III, E. Brucher, S.H. Koenig, A.D. Sherry, M. Spiller, Magn. Reson. Med. 27 (1992) 284.
[53] E. Strandberg, P.-O. Westlund, J. Magn. Reson. series A 122 (1996) 179.
[54] E. Strandberg, P.-O. Westlund, J. Magn. Reson. 137 (1999) 333.
[55] P.-O. Westlund, J. Chem. Phys. 108 (1998) 4945.
[56] T. Nilsson, J. Kowalewski, Mol. Phys. 98 (2000) 1617–1638.
[57] T. Nilsson, J. Kowalewski, J. Magn. Reson. 146 (2000) 345–358.
[58] T. Nilsson, PhD Theses, Stockholm University, 2000.
[59] M. Odelius, C. Ribbing, J. Kowalewski, J. Chem. Phys. 103 (1995) 1800.
[60] M. Odelius, C. Ribbing, J. Kowalewski, J. Chem. Phys. 104 (1996) 3181.
[61] D.M. Brink, G.R. Satchler, Angular Momentum, Oxford University Press, Oxford, 1968.
[62] P.-O. Westlund, H. Wennerström, N. Benetis, Mol. Phys. 61 (1987) 177.
[63] P. Caravan, N.J. Cloutier, M.T. Greenfield, S.A. McDermid, S.U. Dunham, J.W.M. Bulte, J.C. Amedio Jr., R.J. Looby, R.M. Supkowski, W.DeW. Horrocks Jr., T.J. McMurry, R.B. Lauffer, J. Am. Chem. Soc. 124 (2002) 3152.
[64] R.N. Muller, B. Radüchel, S. Laurent, J. Platzek, C. Piérart, P. Mareski, L. Vander Elst, Eur. J. Inorg. Chem. 1999 (1999) 1949.
[65] S.H. Koenig, R.D. Brown III, in: R.K. Gupta, (Ed.), NMR Spectroscopy of Cells and Organisms, vol. 2, CRC Press, Boca Raton, 1987, p. 75.
[66] R. Ruloff, T. Gelbrich, J. Sieler, E. Hoyer, L.Z.N. Beyer, Chem. Sci. 52 (1997) 805.
[67] W. Wang, R.L. Belford, R.B. Clarkson, R.B. Davis, R.B. Forrer, M.J. Nilges, M.D. Timken, T. Watczak, M.C. Thurnauer, J.R. Norris, A.L. Morris, Y. Zwang, Appl. Magn. Reson. 6 (1994) 195.
[68] T.I. Smirnova, A.I. Smirnov, R.L. Belford, R.B. Clarkson, J. Am. Chem. Soc. 120 (1998) 5060.